November 24, 2023

FP20: Magnetooptical trap

Gusti J., Provencio Lameiras, J.C. Tutor: Rautenberg, M.

Contents

1. Data Analysis

1.1 Spectroscopy

During the first part of the experiment, we performed measurements for the Doppler free and the Doppler spectroscopy of Rubidium. We measured the D2 lines ^{87}Rb $F = 2 \to F'$, ^{85}Rb $F = 3 \to F'$, ^{85}Rb $F = 2 \to F'$, and ^{87}Rb $F = 1 \to F'$ both individually and collectively, so that we can calibrate the x-axis with the help of the two ^{87}Rb lines. A transition is possible if it fulfills $\Delta F = 0, \pm 1$, so we have:

$$^{87}\text{Rb } 5S_{1/2},\ F = 2 \to 5P_{3/2},\ F \in \{1, 2, 3\} \tag{1}$$
$$^{85}\text{Rb } 5S_{1/2},\ F = 3 \to 5P_{3/2},\ F \in \{2, 3, 4\} \tag{2}$$
$$^{85}\text{Rb } 5S_{1/2},\ F = 2 \to 5P_{3/2},\ F \in \{1, 2, 3\} \tag{3}$$
$$^{87}\text{Rb } 5S_{1/2},\ F = 1 \to 5P_{3/2},\ F \in \{0, 1, 2\}. \tag{4}$$

1.1.1 Multiplet separation

We can observe the spectrum in Figure 1, where we have included the plot of a quadruple Gaussian function plotted over all of the 4 visible peaks. To determine this fit we used the Doppler-broadened method, since it provided the smoothest Gaussian profiles.

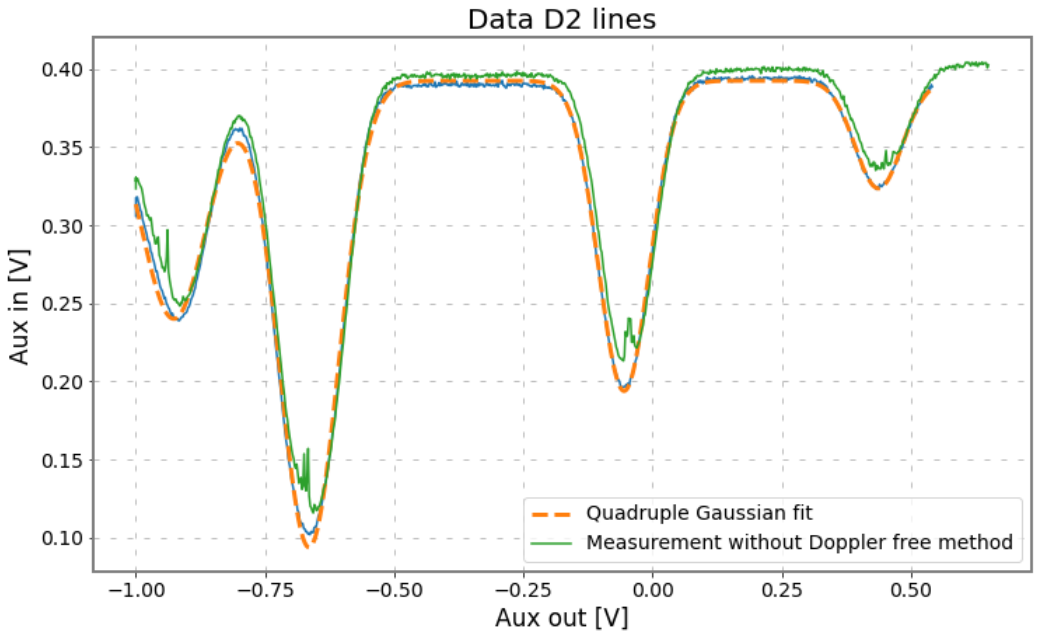

Figure 1: Spectrum of Rubidium, with and without Doppler free spectroscopy method, including a best quadruple Gaussian fit

To calibrate our output, we determined the distance between the two furthermost peaks, corresponding to the ^{87}Rb ground state $5S_{1/2}$ for the values $F = 1$ and $F = 2$ accordingly.

From [2] we obtained the energy separation between the two states, which we will use as our theoretical benchmark for the calibration. We can do this in a simple manner since our axis only has a linear dependence. We will also want to shift the spectrum, so that our ^{87}Rb $5S_{1/2}\,F = 1$ state lies in the 0 position, which is a slightly arbitrary decision but will make the diagramm visually more comprehensible. We can perform the same calculation to try and calibrate our axis with the help of the two ^{85}Rb peaks [1] and then compare the factors with each other.

$$\Delta f_{87} \approx 6.83\,\mathrm{GHz} \tag{5}$$
$$\Delta f_{85} \approx 3.04\,\mathrm{GHz}. \tag{6}$$

We obtain the calibration factors:

$m_{87}\,[\,\mathrm{GHz\,V^{-1}}]$	$m_{87}\,[\,\mathrm{GHz\,V^{-1}}]$	σ
5.01(29)	4.99(62)	0.03

Table 1: Comparison between calibration factors using the $^{87/85}$Rb measurements

where the σ deviation was, and in the following segments will be calculated using

$$\sigma = \frac{|G_1 - G_2|}{\sqrt{(\Delta G_1)^2 + (\Delta G_2)^2}} \tag{7}$$

for two compared values $G_{1,2}$.

With the calibrated horizontal axis, we can more properly draw our plot Figure 2 and determine the frequency of the ^{85}Rb transition, which is given by the distance between the two ^{85}Rb peaks. We measured

$$f_{85,\,F=2\to3} = 3.1(4)\,\mathrm{GHz}. \tag{8}$$

We compare this with a literature taken from [1]

	Measured	Theory	σ
$f_{85}\,[\,\mathrm{GHz}]$	3.1(4)	3.0357324390(60)	0.05

Table 2: Comparison for ground state ^{85}Rb, $F = 2 \to 3$ transition

1.1.2 Natural linewidth and hyperfine splitting

Now we perform a similar analysis for the individual peaks. Our goal is to look into the hyperfine splitting when observing the curve with the Doppler free method, where we can go peak into the excited Rubidium states and compare the measured frequencies with the literature values. The first thing we do is take a look at the measurements

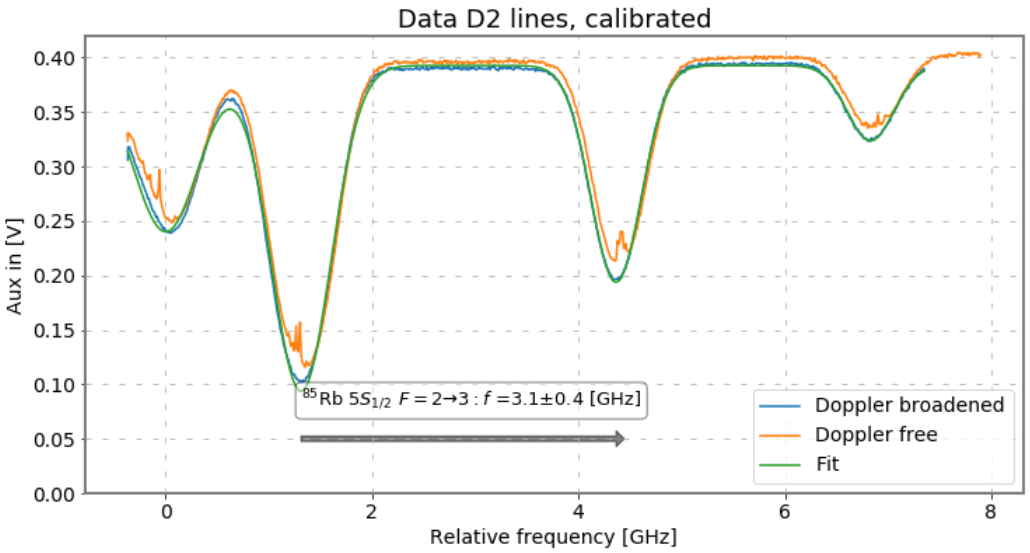

Figure 2: Spectrum of Rubidium, calibrated on its horizontal axis and calculated transition for ground state ^{85}Rb

	$^{85}\mathrm{Rb}_{F=3},\ 2\to4$	$^{87}\mathrm{Rb}_{F=1},\ 0\to2$	$^{87}\mathrm{Rb}_{F=2},\ 2\to3$
$^{85}\mathrm{Rb}_{F=2},\ 1\to3$	23	8	2.6
$^{85}\mathrm{Rb}_{F=3},\ 2\to4$		0.6	9
$^{87}\mathrm{Rb}_{F=1},\ 0\to2$			10

Table 3: Calibration factors for the different transitions

of the individual orders and fit a Gaussian over the Doppler broadened data. We can then substract this Gaussian from the Doppler free data and get a cleaner view into the absorption peaks. This is shown exemplarily for the case of ^{85}Rb $F = 2 \to F'$ **??** and the rest of the diagrams can be seen in the annex to reduce clutter.

As we zoom in into the absorption peaks Figure 4, we can see the structure depicted in Figure 10 of the script [3] and assign the corresponding transitions to the peaks. We do this for each of the peaks in Figure 2 and compare first the calibration factors we calculated. We can see large discrepancies and we will look into possible error sources that could lie behind them.

.

We can also measure the relative frequency separation and compare Table 4 it with literature values found in [1] and [2].

From the comparison we can conclude a couple of things. Firstly, while the sigma deviation between the measurements appears to be quite good, with almost every single value being below 1 σ distance away from the comparison. This would in theory point towards a

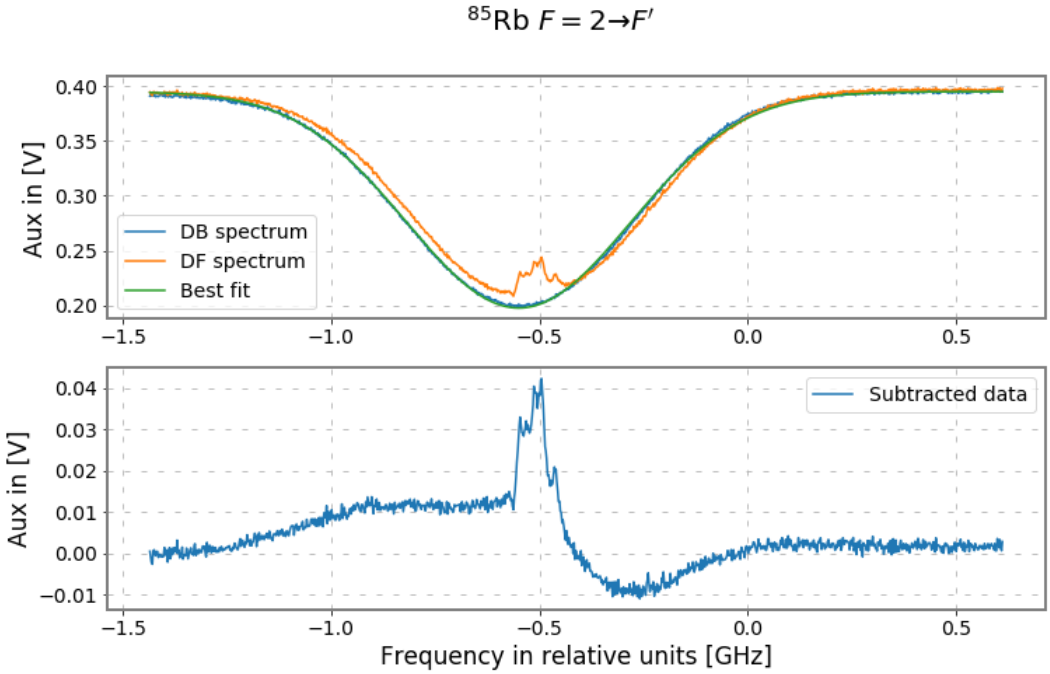

Figure 3: Individual look into the ^{85}Rb $F = 2 \rightarrow F'$ peak, with bare absorption peaks shown as well

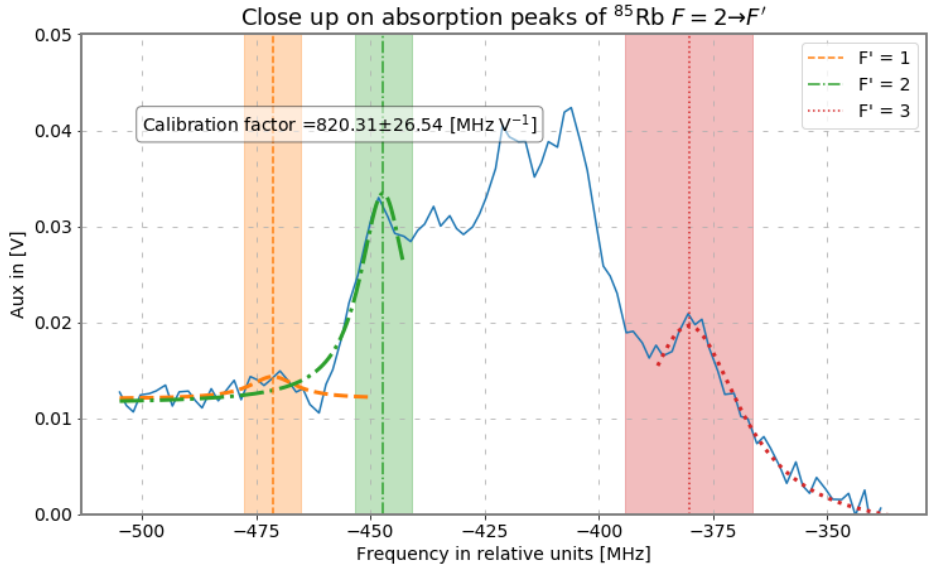

Figure 4: Zoom in into the ^{85}Rb $F = 2 \rightarrow F'$ transitions. The error margin is given by the line width determined by the fit and highlighted with a light band around the determined relative frequency.

proper conductance of the calibration and measurements, however when we take a look at the absolute and relative difference between the literature and the measured values, they

Transition	Lit. [MHz]	Meas. [MHz]	Abs. difference [MHz]	Rel. difference [%]	σ
^{85}Rb $F: 1 \to 2$	29.37(9)	24(9)	5	18	0.6
^{85}Rb $F: 2 \to 3$	63.40(6)	70(15)	7	10	0.2
		40(15)	33	75	0.7
^{85}Rb $F: 3 \to 4$	120.64(7)	140(30)	19	16	0.6
^{87}Rb $F: 0 \to 1$	72.418(6)	95(25)	23	31	0.9
^{87}Rb $F: 1 \to 2$	159.947(7)	135(21)	25	16	1.2
^{87}Rb $F: 2 \to 3$	266.650(9)	265(11)	2	0.6	0.15

Table 4: Relative frequency separation between spectral lines

portray a different story. The measurements are in reality quite far off from each other, but the disproportionally large deviations of the measured values, which we got from the peak widths, give the impression of a better concordance between results.

2. Loading curves

Now we want to analyse the loading curves of the MOT. We must include first of all a brief disclaimer, that during our execution of the experiment we weren't able to find a MOT that was appropriate enough for the measurement, which is why we will borrow data from a different group. The data was found under the folder "NikolasJohann" in the experiment PC. It was picked because it had better than the remaining groups documented the measurement parameters under which every measurement had been performed, for example stating the AOM frequency and the current gradient in the name of the files themselves. Since we were not able to contact any group with the measurements for a proper documentation, we had to interpolate from the file names a lot of necessary information. For example, during our execution, the AOM frequency displayed in the monitor was slightly offset from the one displayed on the instrumentation. Since we have no basis upon which to judge what the real value is, based on the filenames alone, we will use them with caution and having in mind that there can be some fluctutations in the data and the reality.

The first step we want to undertake is to convert the voltage signal from the photodetector into the number of atoms. On top of the data we will fit a function that describes the rate equation (VIII.2.1 in script)

$$\frac{\mathrm{d}N}{\mathrm{d}t} = L - \alpha N. \tag{9}$$

This differential equation can be easily solved by

$$N(t) = \frac{L}{\alpha} + c_1 \mathrm{e}^{-\alpha t}. \tag{10}$$

If we assume that $N(0) = 0$, then we also get the result $c_1 = -\frac{L}{\alpha}$. In practice this isn't apparently the case with the data at hand, especially since we don't have a background measurement to substract from our analysis. Instead, we will work with an unknown variable N_0 and try to proceed analogously with

$$N(t) = \frac{L}{\alpha}\left(1 - \mathrm{e}^{-\alpha t}\right) + N_0. \tag{11}$$

We also need to convert the signal into the number of atoms, which we can do per the script (IV.8.1) with the scattering rate of the atoms γ_{sc} and some other pieces of information:

$$\gamma_{sc}(\Delta) = \frac{\gamma}{2} \cdot \frac{I(r)/I_{sat}}{1 + I(r)/I_{sat} + 4\Delta^2/\gamma^2} \tag{12}$$

where we take the natural linewidth $\gamma = \gamma(^{85}\mathrm{Rb}) = 2\pi 6.07\,\mathrm{MHz}$ and the saturation intensity $I_{sat} = 4.1\,\mathrm{mW\,cm^{-2}}$. This formula depends on the detuning of the lasers Δ, which can be determined as in the script (VII.2.1). We will also approximate $I(r)$ with I_0 for the intensity at the center of the beam. Since we are using foreign data for this measurement, and we weren't able to contact the original sources for further information, we will take a placeholder value, estimated by the value our tutor mentioned we should strive for: $P_{\mathrm{PWMT}} = 20\,\mathrm{mW}$. The intensity I_0 can be given as $I_0 = \frac{2P_{\mathrm{PWMT}}}{\pi w^2}$ with a Gaussian beam with a waist $w = 2$ mm.

We account as well for the isotropic sponteaneous emission:

$$P_{\mathrm{emitted}} = \gamma_{sc}(\Delta) E_\nu(\lambda) N_{\mathrm{atoms}} \tag{13}$$

with $E_\nu(\lambda) = hc/\lambda$. Finally, we account for the smaller spatial angle where we can detect atoms in the first place. $P_{\mathrm{meas}} = \theta_\Omega P_{\mathrm{emitted}}$ with $\theta_\Omega = \frac{\pi r^2}{4\pi d^2} = \frac{\pi(25.4\mathrm{mm})^2}{4\pi(150\mathrm{mm})^2}$. Finally, since we don't measure power with our detector, but a voltage, we need to convert this into a measured power. The script mentions we should use the "conversion table", which as such doesn't appear in the mentioned manual, as neither does the mentioned resistor of "10 MOHM". Instead, we assume that we can determine the power using the responsivity (Res $= I/P$) and transform the voltage to a current using the specified resistance of $R = 50\Omega$ to get the power. We can see in the diagram (manual, 6.1) that for $\lambda \approx 800\,\mathrm{nm}$ the responsivity for infrared light is roughly $\mathrm{Res} = 0.5\,\mathrm{A\,W^{-1}}$ We pick this value because the ^{85}Rb D lines are in this range.

In total we will have to perform the following conversion:

$$
\begin{aligned}
N_{\text{atoms}} &= \frac{P_{\text{emitted}}}{\gamma_{\text{sc}}(\Delta)E_\nu(\lambda)} = \frac{P_{\text{meas}}/\theta_\Omega}{\gamma_{sc}E_\nu} \qquad (14)\\
&= \frac{\frac{I}{\text{Res}\,\theta_\Omega}}{\gamma_{sc}E_\nu}\\
&= \frac{U}{\gamma_{sc}} \cdot \frac{1}{R\,\text{Res}\,\theta_\Omega E_\nu}
\end{aligned}
$$

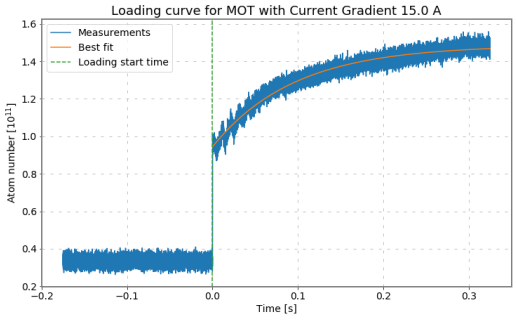

Figure 5: Loading curve for a current gradient of 15 A

with the measured voltage U and the previously mentioned values. For the energy $E_\nu(\lambda)$ we will use the wavelength of the $D1$ line of ^{85}Rb, as we would expect this is roughly the wavelength that reaches the photodetector. We can now fit (11) on the data and determine the loading and the loss rate in dependency of the detuning and the current gradient. We will show exemplarily one plot for each of the parameters (detuning Figure 6 and current gradient Figure 5) and the final result. The rest can be seen in the annex.

We did this in total for the AOM frequencies $107, 109, 111, 112$ and $116\,\text{MHz}$ and for the current gradients $14, 14.5, 15, 15.5, 16\,\text{A}$. Here it will be clear from (VII.2.1), that an AOM frequency of $116\,\text{MHz}$ returns a positive detuning. For a laser with a negative detuning, the atoms cool off since they emit light with a higher frequency than with which the state changes were exited in the first place. A positive detuning would mean, that for every emission, more energy is input into the system than is leaving, which would heat the sample instead. This doesn't make sense, which leads us to the conclusion that there is a systematic error in the documentation of the measurements. During our execution, we could see that the values in the monitor and the instrumentation were offest by roughly $2\,\text{MHz}$, which would bringt the $116\,\text{MHz}$ to the valid $114\,\text{MHz}$. We decide at this point actively against a revision of the diagram documentations, since we can't with certainty speak for the conditions of the original source's execution. We will however, have this in mind during the discussion.

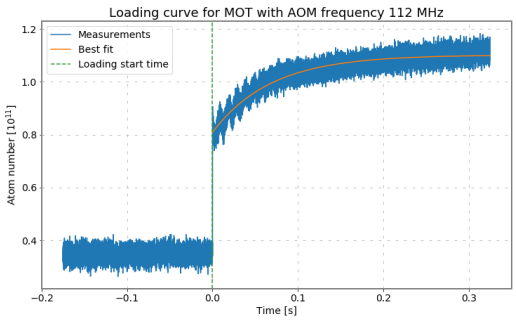

Figure 6: Loading curve for a stated AOM frequency of 112 MHz, implying a detuning of $-6\,\text{MHz}$

From the measurements we can determine the loading and the loss rate, which can be seen in Figure 7 and Figure 8

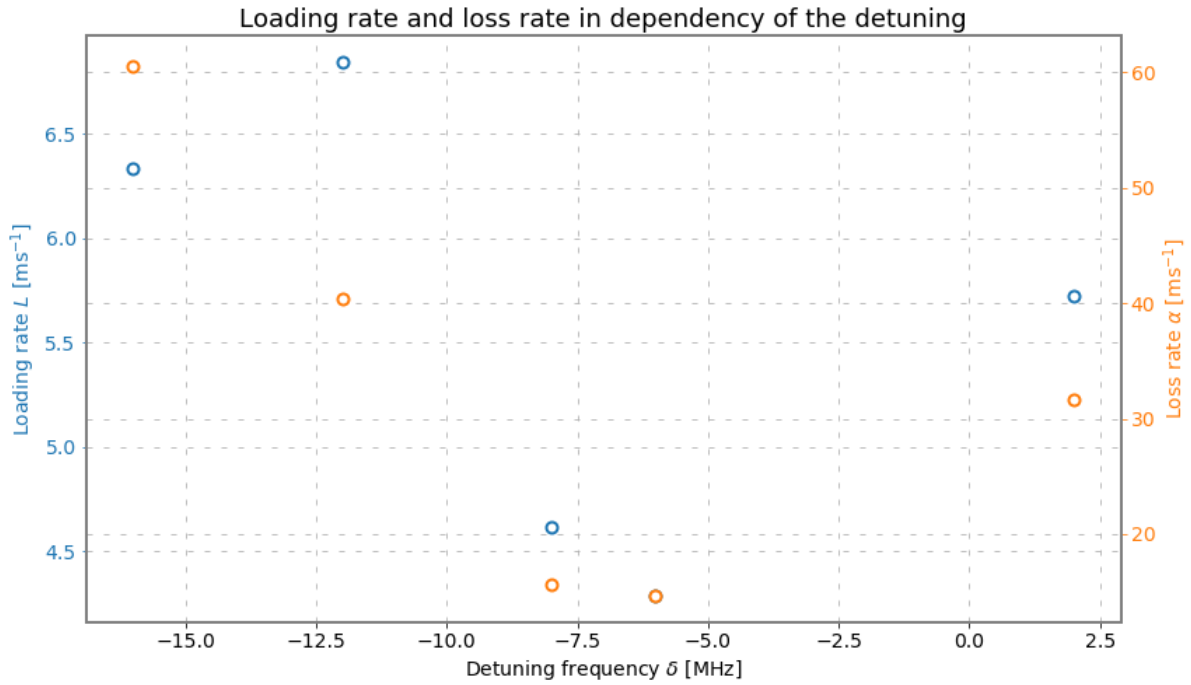

Figure 7: Loading and loss rate for different laser detunings, we can see the outlier value at a positive detuning frequency which doesn't make physical sense as discussed previously

One can expect to see a peak in the number of atoms, because the force on the atoms is maximised when the detuning is equal to the negative Doppler frequency as per (IV.1.2).

3. Release and recapture

For the final part of our evaluation, we want to determine the temperature of the probe by applying the release and recapture method. Here, we will load the MOT so that it has a stable maximum amount of atoms, then quickly turn off the cooling light and let the atom cloud expand freely, where some of the atoms will gain enough energy to leave the trap. After a certain time, we will turn on the cooling atoms and compare how many are still left. We will take into account the off-time as the zero-atom level and subtract this from our measurements of the maximum and the recaptured amount. An example for this can be seen in Figure 9.

We do this successively for every measurement available and determine the mean number of atoms in the maximum range, and in an arbitrary range after recapturing. We choose a sample of 100 data points for the latter, so as not to step too far into the range where too many atoms have been recaptured. We can see in Figure 10 that the measurements quite neatly align with our expectation. Especially, considering that the calculated temperature

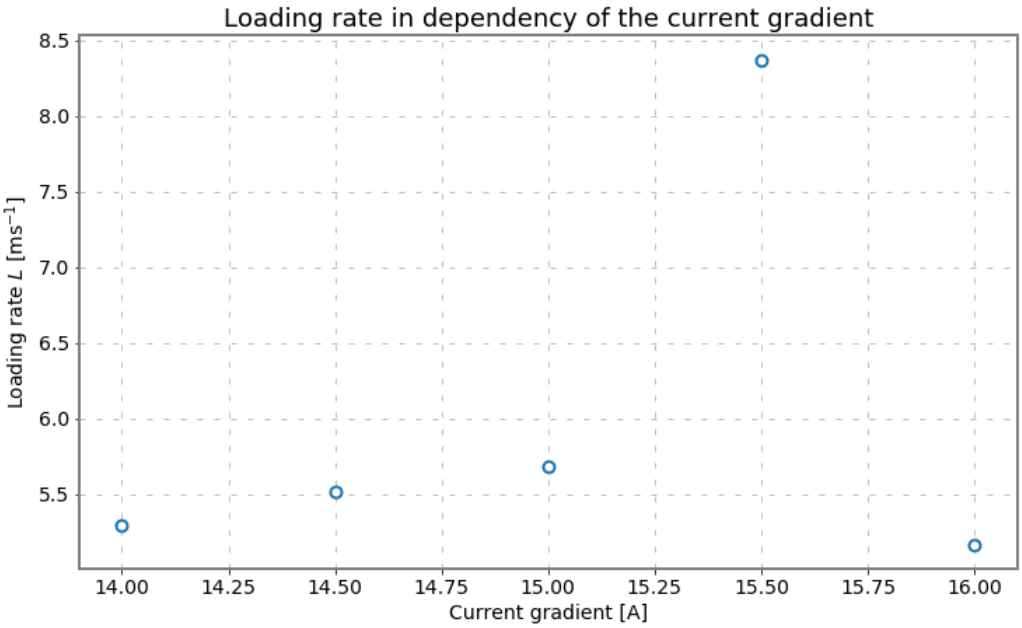

Figure 8: Loading rate for different current gradients

of $T = 186.515(4)\,\mu$K lies above the Doppler temperature $T_d = 145.57\,\mu$K, which is the larger of the theoretical limits. The error was calculated as the squared root of the covariance for the fit.

For some concluding remarks, we want to discuss possible sources for error. The biggest one, despite being redundant, is the fact that we're using external data for which we had to make very broad assumptions and interpolations, since we didn't know many of the important parameters that we needed to take into account and at many steps replaced with placeholder values for the sake of continuing with the evaluation. This fact alones invalidates any conclusion we could possibly get from the results.

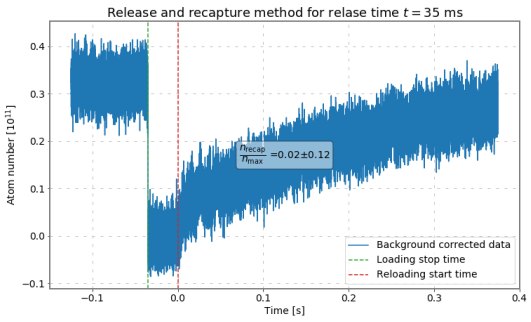

Figure 9: Release and recapture method for a downtime of $t = 35$ ms. This is the longest the MOT was off in the data we have available

Another source for error, related also to the data at hand is, that for most of the measurements in part 2 no background measurements were performed, which affects our evaluation significantly.

Perhaps most importantly, a source for error could be the bees that are kept on the roof

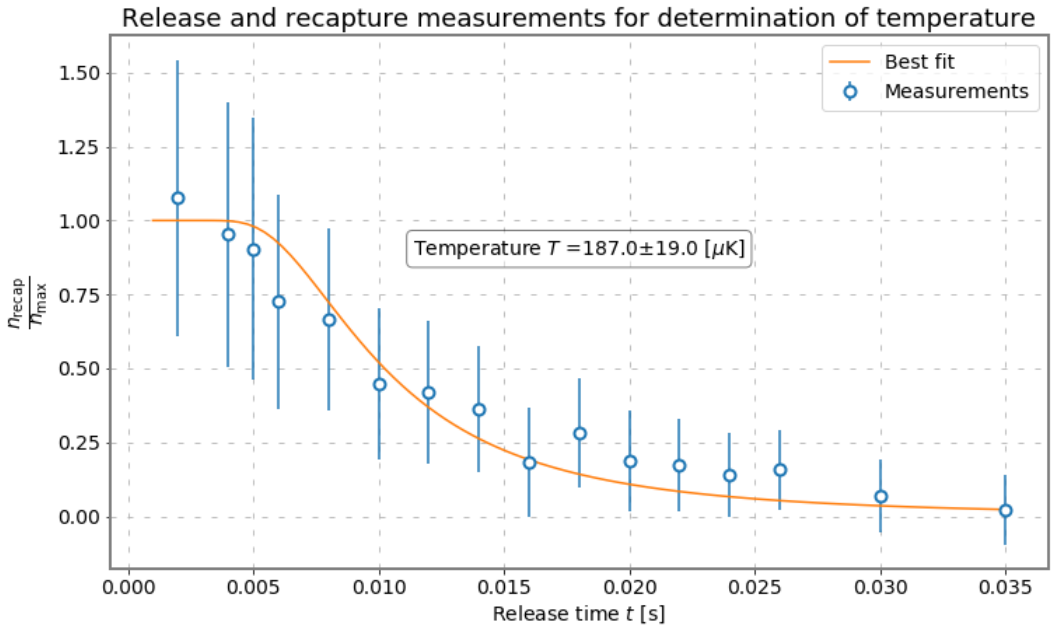

Figure 10: Determination of the temperature with the help of the release and recapture method

of the Physic's Institut, since their constant buzzing introduces vibrations which affect the instrumentation.

4. Annex

4.1 Natural linewidth and hyperfine splitting

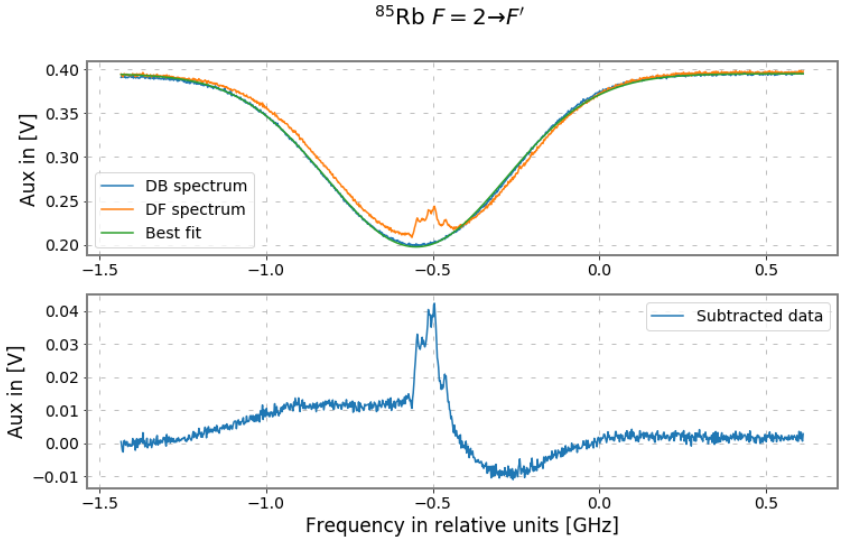

Figure 11: Individual look into the ^{85}Rb $F = 2 \rightarrow F'$ peak, with bare absorption peaks shown as well

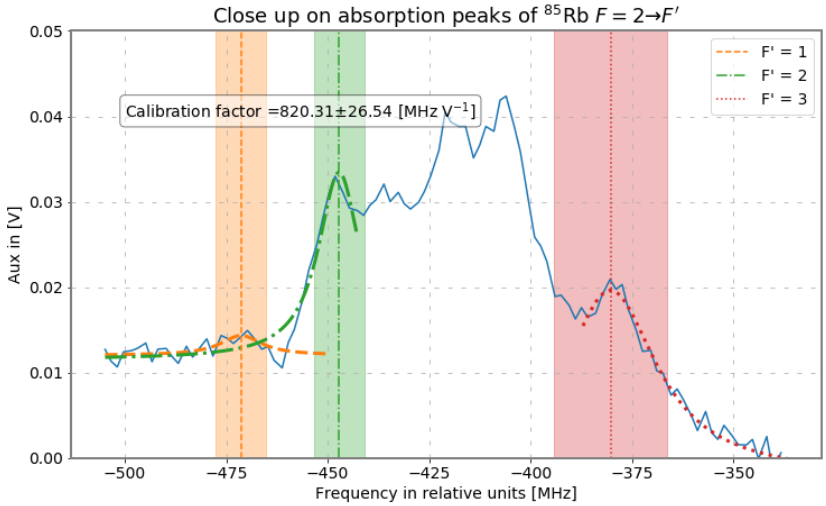

Figure 12: Zoom in into the ^{85}Rb $F = 2 \rightarrow F'$ transitions. The error margin is given by the line width determined by the fit and highlighted with a light band around the determined relative frequency.

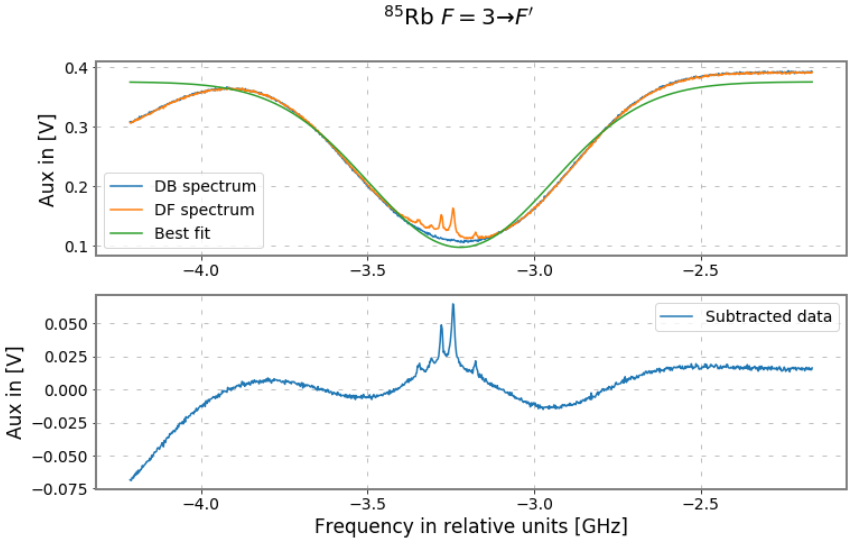

Figure 13: Individual look into the ^{85}Rb $F = 3 \rightarrow F'$ peak, with bare absorption peaks shown as well

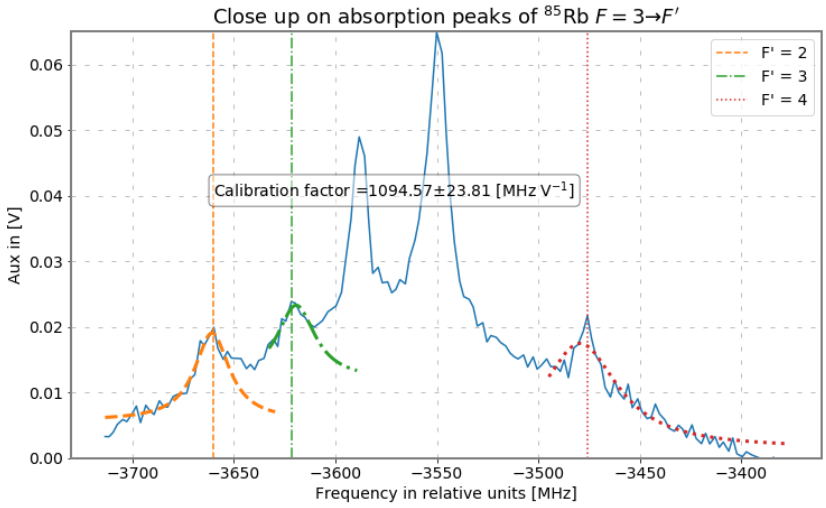

Figure 14: Zoom in into the ^{85}Rb $F = 3 \rightarrow F'$ transitions. The error margin is given by the line width determined by the fit.

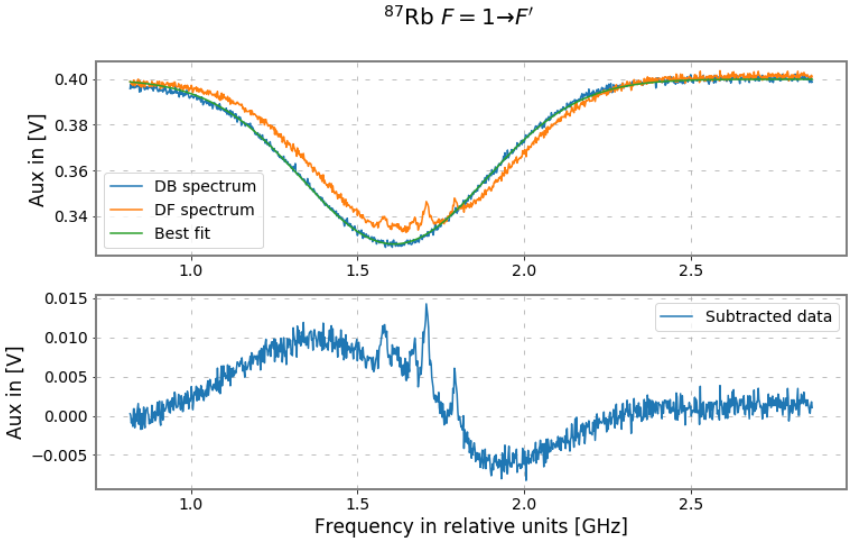

Figure 15: Individual look into the ^{87}Rb $F = 1 \rightarrow F'$ peak, with bare absorption peaks shown as well

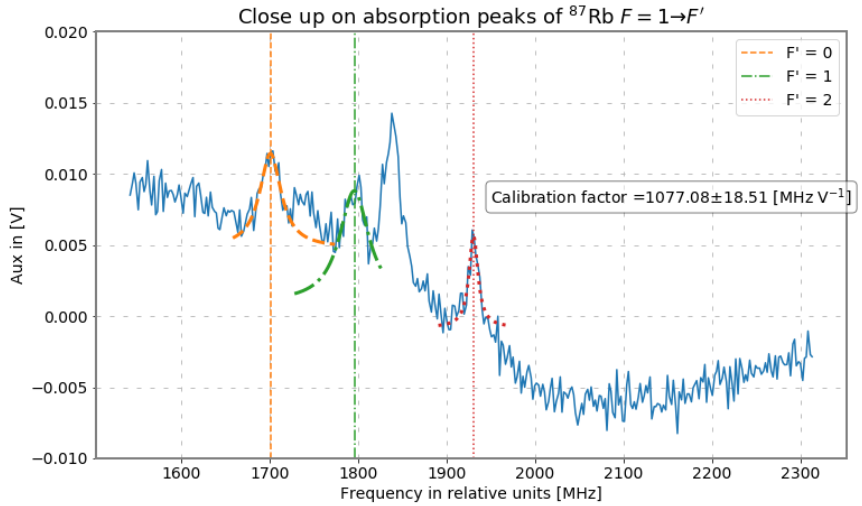

Figure 16: Zoom in into the ^{87}Rb $F = 1 \rightarrow F'$ transitions. The error margin is given by the line width determined by the fit.

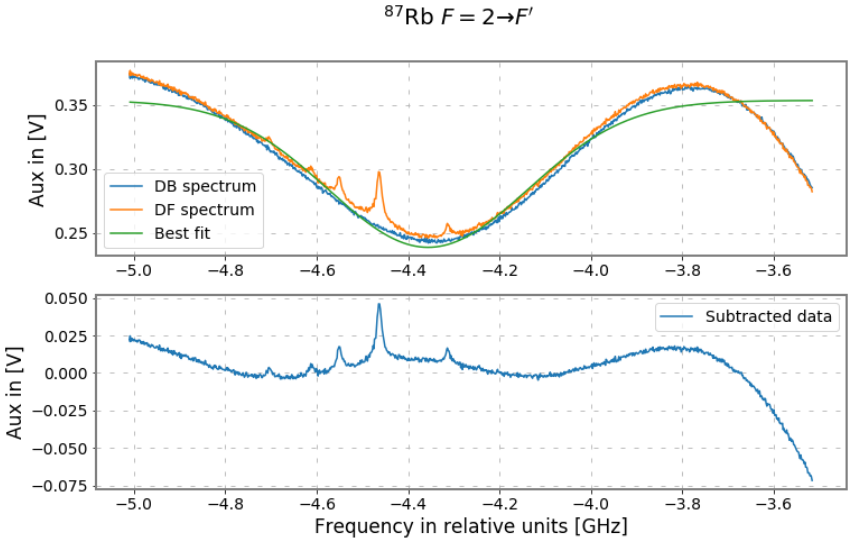

Figure 17: Individual look into the ^{87}Rb $F = 2 \rightarrow F'$ peak, with bare absorption peaks shown as well

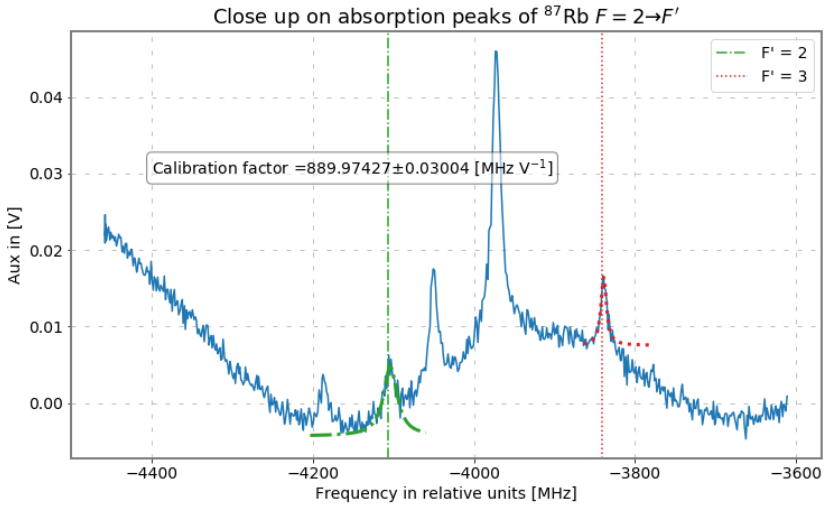

Figure 18: Zoom in into the ^{87}Rb $F = 2 \rightarrow F'$ transitions. The error margin is given by the line width determined by the fit.

4.2 Loading curves

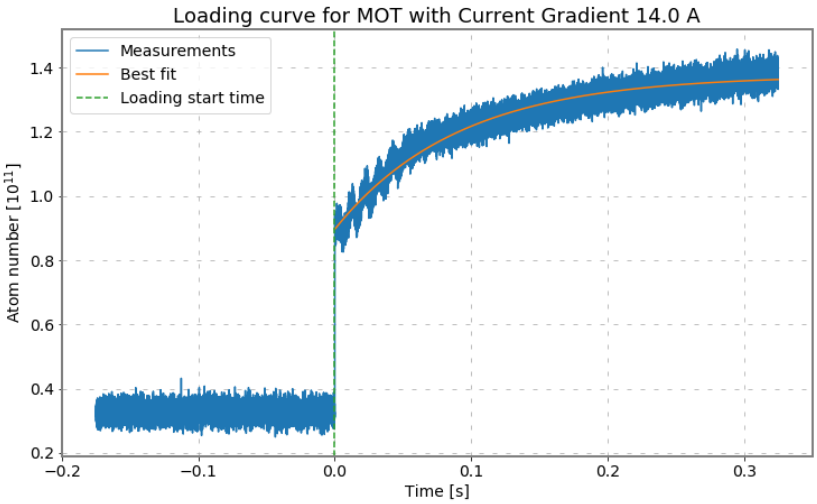

Figure 19: Loading curve for a current gradient of 14 A

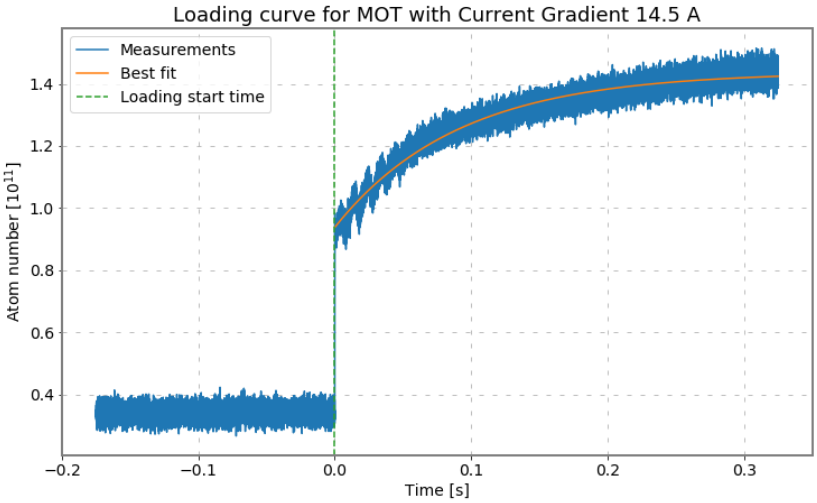

Figure 20: Loading curve for a current gradient of 14.5 A

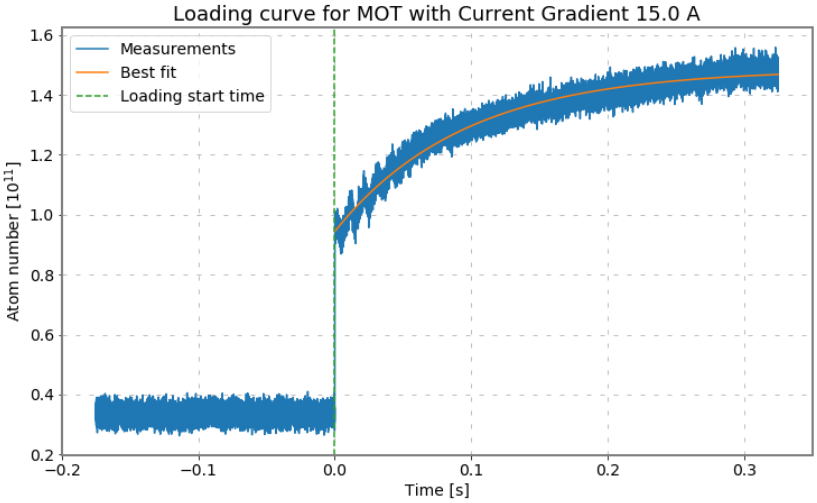

Figure 21: Loading curve for a current gradient of 15 A

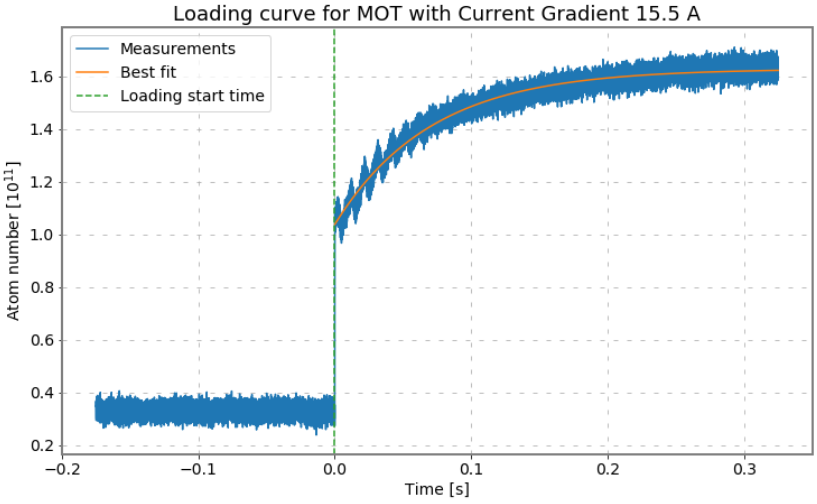

Figure 22: Loading curve for a current gradient of 15.5 A

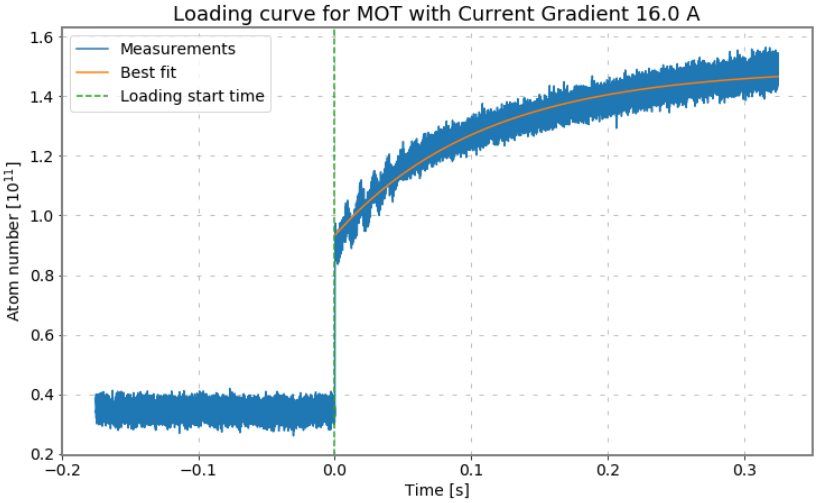

Figure 23: Loading curve for a current gradient of 16 A

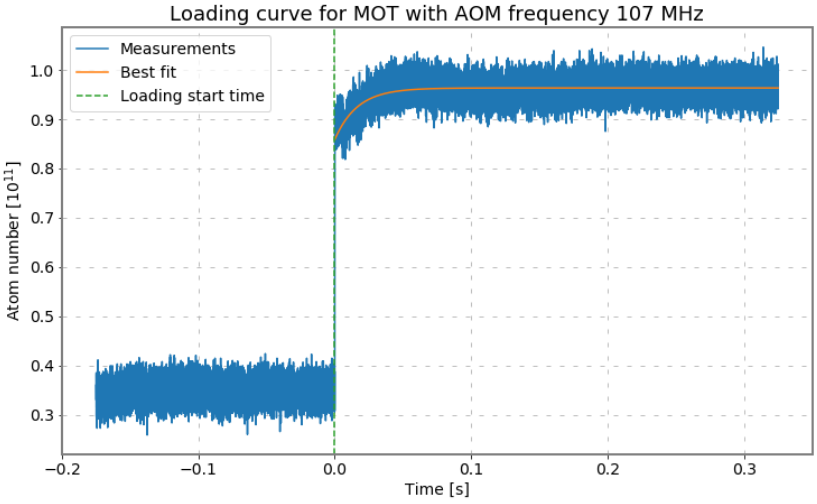

Figure 24: Loading curve for a stated AOM frequency of 107 MHz

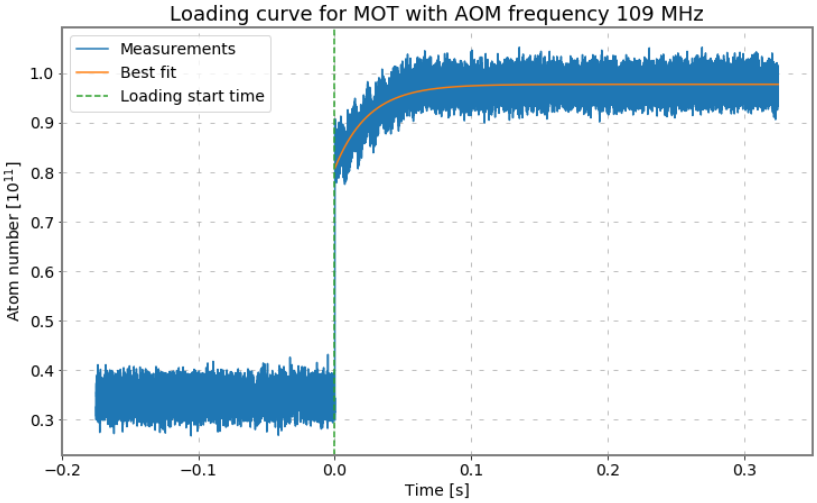

Figure 25: Loading curve for a stated AOM frequency of 109 MHz

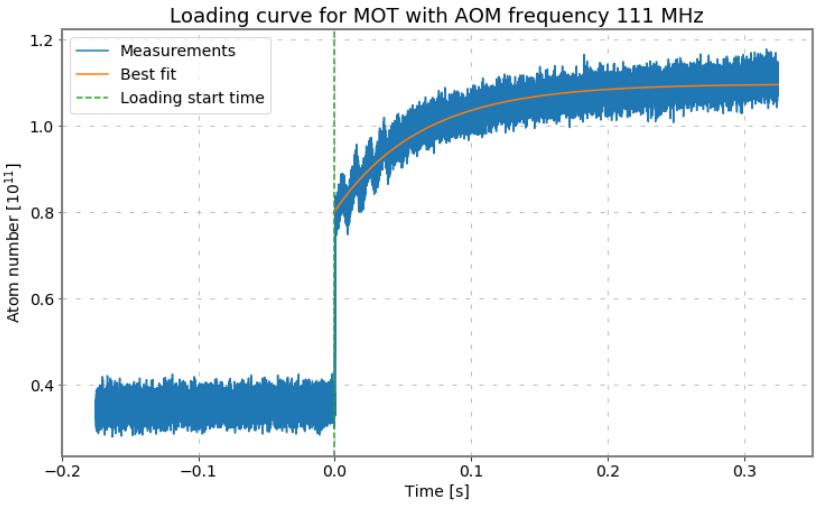

Figure 26: Loading curve for a stated AOM frequency of 111 MHz

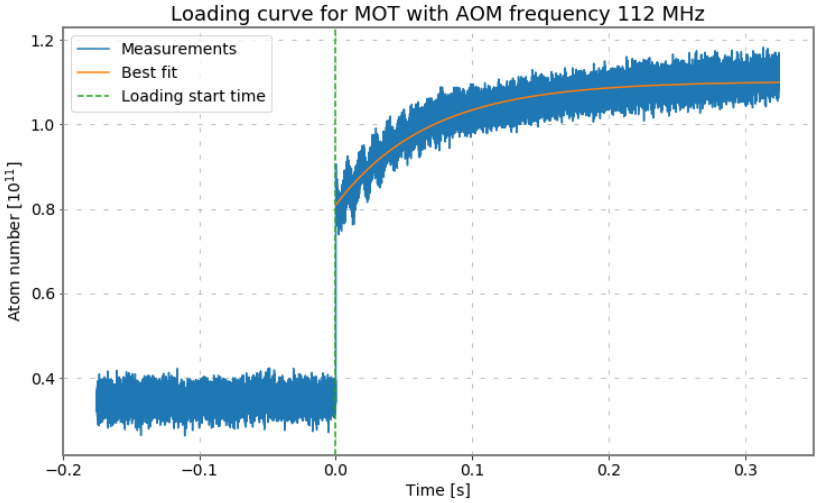

Figure 27: Loading curve for a stated AOM frequency of 112 MHz

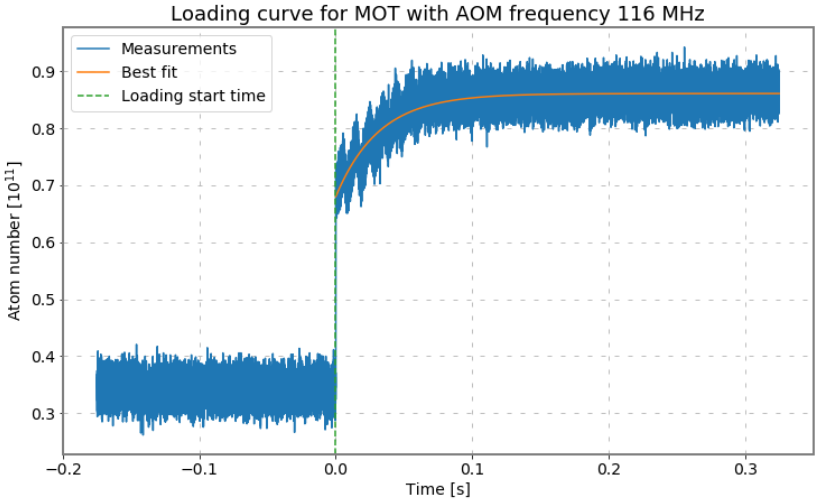

Figure 28: Loading curve for a stated AOM frequency of 116 MHz

References

[1] Daniel Steck. *Rubidium 85 D Line Data*. URL: https://steck.us/alkalidata/rubidium85numbers.pdf.

[2] Daniel Steck. "Rubidium 87 D Line Data". In: *Steck.us* (). URL: https://steck.us/alkalidata/rubidium87numbers.1.6.pdf.

[3] FP Tutors. *FORTGESCHRITTENEN-PRAKTIKUM VERSUCH: PREPARATORY MATERIAL - Magneto-optische Falle*. URL: https://www.physi.uni-heidelberg.de/Einrichtungen/FP/anleitungen/F20.pdf.